Synchrony of African rainforest solar induced chlorophyll fluorescence and environmental factors

Russell Doughty[1*], Michael C. Wimberly[2], Dan Wanyama[2], Helene Peiro[1,3], Nicholas Parazoo[4], Sean Crowell[5], Moses Azong Cho[6]

[1]College of Atmospheric and Geographic Sciences, University of Oklahoma, Norman, OK, 73019, USA
[2]Department of Geography and Environmental Sustainability, University of Oklahoma, Norman, OK, 73019, USA
[3]Netherlands Institute for Space Research (SRON), Leiden, The Netherlands
[4]Jet Propulsion Laboratory, California Institute of Technology, Pasadena, CA 91109, USA
[5]LumenUs Scientific Solutions, LLC, Oklahoma City, Oklahoma.
[6]Precision Agriculture Research Group, Advanced Agriculture and Food, CSIR, Pretoria, South Africa

Correspondence to: Russell Doughty (russell.doughty@ou.edu)

Abstract. Global atmospheric carbon dioxide concentrations are largely driven by terrestrial photosynthesis, of which tropical forests account for one third. Relative to other tropical regions, less is known about the seasonality of African tropical forest productivity and its synchrony with environmental factors due to a lack of in situ carbon flux data. To help fill this knowledge gap, we use spaceborne solar-induced chlorophyll fluorescence (SIF), vegetation indices, and climate data to investigate the seasonality and synchrony of photosynthesis in Africa's tropical forest ecoregions. We find West African SIF to increase during the dry season and peak prior to precipitation, as has been observed in the Amazon. In Central Africa, we find a continental-scale bimodal seasonality in SIF, the minimum of which is synchronous with precipitation, but its maximum is likely less related to environmental drivers.

1 Introduction

The intra- and inter-annual variability of global atmospheric carbon dioxide concentration is driven largely by changes in the terrestrial uptake of carbon dioxide through photosynthesis, and tropical forests are playing an increasingly important role in this variability (Wang et al., 2014). Tropical forests account for about one-third of global photosynthesis, house one half of Earth's terrestrial carbon store, and sequester about 15% of anthropogenic carbon dioxide emissions (Gaubert et al., 2019; Pan et al., 2011; Sitch et al., 2015). They also play important roles in the global water cycle via precipitation recycling and cloud formation (Lawrence and Vandecar, 2015; Spracklen et al., 2012). Thus, tropical forests are critical to regulating global climate.

Relative to the Amazon basin of South America, less is known about the seasonality of photosynthesis of African tropical forests, their drivers, and their responses to changes in climate due to a lack of eddy covariance tower measurements in structurally intact forests (Malhi, 2012; Merbold et al., 2009; Williams et al., 2007). Responses of African tropical forest productivity to climate have instead been gleaned from syntheses of (1) field plot measurements that have focused on changes

32 in aboveground biomass to assess carbon gains, losses, and the net carbon sink over the three decades preceding 2015; and (2)

33 satellite remote sensing of leaf area and greenness.

34 Studies that have focused on field plot measurements had three main findings. First, they found a significant upward trend in

35 carbon gains (Hubau et al., 2020) that were unaffected by anomalously low precipitation and high temperatures during the

36 2015/2016 El Nino (Bennett et al., 2021). Second, there was no significant trend in carbon losses, which were also not

37 significantly affected by the 2015/2016 El Nino, despite there being a strong correlation between precipitation and the net

38 carbon sink at the continental scale (Williams et al., 2007). Finally, there was no significant trend in the net carbon sink, but

39 that the net sink, which remained positive, was significantly reduced by the 2015/2016 El Nino. Thus, field-based evidence

40 suggests that African tropical forests are especially resistant and resilient to climate extremes.

41 The satellite remote sensing studies have noted a double peak in the seasonality of leaf area and greenness in the Congolian

42 tropical forests, which is synchronous with precipitation, but little has been published on these seasonalities for West African

43 tropical forests. What has been debated is whether there is a significant long-term browning trend in Congolian tropical forests

44 (Zhou et al., 2014) that accompanies observed large-scale and long-term drying (Asefi-Najafabady and Saatchi, 2013; Jiang et

45 al., 2019; Malhi and Wright, 2004), but the most recent study to address this trend found no widespread long term decline in

46 leaf area or greenness (Sun et al., 2022). This latest finding supports field observations that have found no significant trend in

47 the net carbon sink, and further suggests that African tropical forests have been relatively insensitive to changes in climate.

48 Although these studies have investigated long-term changes in the net carbon sink, greenness, and leaf area, they provide little

49 insight into the relationship between photosynthesis and environmental factors or how photosynthesis responds to climate

50 anomalies. For instance, the field investigations do not provide definitive evidence for whether the decrease in the net carbon

51 sink during the 2015/2016 El Nino was due to decreased photosynthesis, increased respiration, or both. Also, these previous

52 field-based analyses aggregated measurements annually at the continental scale and the field sampling was more commonly

53 conducted in coastal forests (Blundo et al., 2021; Lopez-Gonzalez et al., 2011), which tend to have higher annual total rainfall

54 and extreme variability in monthly precipitation and photosynthetically active radiation (PAR) compared to the interior

55 Congolian rainforest.

56 Recent advancements in the retrieval of solar-induced chlorophyll fluorescence (SIF) from space provides an observation-

57 based method for monitoring plant physiology and the amount of PAR absorbed by chlorophyll ($APAR_{chl}$) and has been

58 described as a proxy of photosynthesis (Doughty et al., 2019, 2021b). SIF is a small amount of energy that is re-emitted by

59 chlorophyll (1%-2%) and is sensitive to leaf physiology (Johnson and Berry, 2021; Porcar-Castell et al., 2021, 2014). Thus,

60 SIF is directly sensitive to changes in $APAR_{chl}$ and can correlate to changes in photosynthetic activity (Yang et al., 2018),

61 particularly at coarse spatio-temporal resolutions (Magney et al., 2020). For example, spaceborne SIF was found to mimic the

62 seasonality of photosynthesis estimated at eddy covariance tower sites in the tropical Amazon forest, and more closely tracked

63 photosynthesis than vegetation indices (Doughty et al., 2019), which have traditionally been used to estimate $APAR_{chl}$ and to

64 model photosynthesis globally (Pei et al., 2022).

65   The studies that have utilized spaceborne SIF to investigate tropical Africa have found that (1) temperature and vapor pressure

66   deficit (VPD) control the productivity of African tropical forests (Madani et al., 2017; Umuhoza et al., 2023); (2) SIF tracks

67   well the seasonality of photosynthesis, or gross primary productivity (GPP), over Africa (Mengistu et al., 2021); and (3) SIF

68   has weak to insignificant relationships with VIs and VI-based $APAR_{chl}$ (Doughty et al., 2021b). However, these earlier remote

69   sensing studies have not characterized the relationships between SIF and environmental factors for African tropical forests at

70   regional scales despite there being important and substantial differences in the seasonalities and variability of environmental

71   factors. Relatively high spatial resolution spaceborne SIF data acquired from the newest SIF platforms, including TROPOMI,

72   OCO-2, and OCO-3, is now available and allows us to characterize the relationships between SIF and environmental factors

73   at finer spatial scales.

74   Here, we leverage SIF data from these platforms to advance our knowledge on African tropical forest carbon uptake by

75   inferring the seasonality of photosynthesis for 11 African tropical forest ecoregions from 2019 through 2021. Photosynthesis

76   and SIF was found to be decoupled from vegetation indices and precipitation in the Amazon due to changes in leaf demography

77   and physiology (Doughty et al., 2019; Restrepo-Coupe et al., 2013; Wu et al., 2016). An analysis of six subtropical evergreen

78   species in Africa found the correlation between VIs and leaf nutrients, which are closely related to photosynthesis, to be

79   seasonally dependent (Van Deventer et al., 2015). Also, studies have found tropical moist forests with more than 2000 mm

80   mean annual precipitation (MAP) to be radiation-limited rather than water-limited (Doughty et al., 2019; Guan et al., 2015),

81   and that photosynthesis and SIF of moist Amazon forests were positively associated with VPD (Green et al., 2020).

82   Thus, we suspected that leaf demography and physiology could be responding similarly in moist African tropical forests to

83   changes in environmental conditions. Our first hypothesis was that the seasonalities of SIF and vegetation indices in ecoregions

84   with moist forest (> 2000 mm MAP) would differ substantially but would be more highly correlated in less moist forest (<

85   2000 mm MAP). Our second hypothesis was that SIF would be more strongly coupled with precipitation in less moist African

86   forests and that SIF and VPD would be positively correlated in moist forest.

87   **2 Methods**

88   **2.1 OCO-2 and OCO-3 SIF**

89   The Orbiting Carbon Observatory-2 (OCO-2) is a NASA satellite that was launched in July 2014, and OCO-3 is a duplicate

90   of the OCO-2 grating spectrometer that was attached to the Japanese Experimental Module Exposed Facility (JEM-EF) on the

91   International Space Station (ISS) in May 2019 (Eldering et al., 2019). They have three bands: an oxygen-A band at 0.765 μm

92   and carbon dioxide bands at 1.61 μm and 2.06 μm. The swath widths are ~10 km with eight measurements across-track. The

93   spatial resolution at nadir is slightly different for OCO-2 and OCO-3, about 1.3 km by 2.25 km and 1.6 km by 2.2 km,

94   respectively.

95   We used the ungridded, sounding-level data from the Level 2 v10 SIF Lite files that are available for each platform (OCO-2

96   Science Team et al., 2020; OCO-3 Science Team et al., 2020). We used SIF scaled to 740 nm, which is computed using

97   retrievals from the 757 nm and 771 nm spectral windows and a reference spectral shape for SIF (Doughty et al., 2021a). Scaling

98   to 740 nm can reduce uncertainty and allows for a better comparison among sensors as the various sensors from which we

99   retrieve SIF have different retrieval windows. Also, we used daily adjusted values, which are scaled from instantaneous SIF

100   values using the geometry of incoming solar radiation for that day to help account for differences in the timing of data

101   acquisition and solar illumination angles (Frankenberg et al., 2011; Köhler et al., 2018).

2.2 TROPOMI SIF

103   The TROPOspheric Monitoring Instrument (TROPOMI) instrument is on board the Copernicus Sentinel-5 Precursor satellite,

104   which launched in October 2017. It provides near-daily global SIF data since May 2018 at a resolution of 3.5 km by 5.5 km at

105   nadir and has a swath width of ~2600 km. Here we used the Level 2 TROPOspheric Monitoring Instrument (TROPOMI)

106   TROPOSIF data product (Guanter et al., 2021). We used daily averaged SIF retrievals from the 743-758 nm retrieval window

107   as the 735-758 nm window had a higher sensitivity to atmospheric effects (Guanter et al., 2021). These data are also scaled to

108   740 nm values. We did not filter any of the SIF data from OCO-2, OCO-3, or TROPOMI using a cloud fraction threshold as

109   SIF is relatively less sensitive to cloud cover than surface reflectance (Guanter et al., 2015) and we wanted to avoid a clear sky

110   bias (Köhler et al., 2018).

2.3 CHIRPS Precipitation

112   Climate Hazards group InfraRed Precipitation with Stations (CHIRPS) is a long-term, near-global, daily data set. CHIRPS

113   incorporates The Climate Hazards Group climatology (CHPclim), 0.05° resolution satellite imagery, and in-situ station data

114   to produce a 0.05° resolution gridded data set for time series, trend, and drought monitoring (Funk et al., 2015).

2.4 ERA5 Reanalysis

116   We used monthly averaged data from the ERA5-Land product (Muñoz Sabater, 2019), which is available in a spatial resolution

117   of 0.1 degrees, for air temperature, photosynthetically active radiation (PAR) at the top of the canopy (PAR$_{TOC}$), VPD, and

118   volumetric soil moisture. PAR$_{TOC}$ was calculated as a fraction (0.48) of the downward shortwave radiation from ERA5 after

119   being converted from J/m-2 to W/m-2 by dividing the original values by the number of seconds in the month. VPD was

120   calculated by first applying Tetens equation to air temperature (T_{air}) and dew point temperature (T_{dew}) for temperatures above

121   0°C (Monteith and Unsworth, 2013):

$$es = 0.61078 \times exp(\frac{17.267T_{air}}{237.3+T_{air}}) \tag{1}$$

$$ea = 0.61078 \times exp(\frac{17.267T_{dew}}{237.3+T_{dew}}) \tag{2}$$

124   where es is the saturation vapor pressure or vapor pressure at air temperature, and ea is the actual vapor pressure or vapor

125   pressure at dew point temperature. VPD was then derived as:

$$VPD = es - ea \tag{3}$$

4

2.5 MODIS Surface Reflectance and Vegetation Indices

We used the 500-m daily MCD43A4 surface reflectance product (Schaaf and Wang, 2015) to compute four vegetation indices: the Normalized Difference Vegetation Index (NDVI), Enhanced Vegetation Index (EVI), the Near-infrared Reflectance of Vegetation (NIRv), and the Land Surface Water Index (LSWI). NDVI has been traditionally used to assess vegetation greenness (Rouse et al., 1974), but it tends to saturate in areas with a high leaf area index such as the tropics (Huete et al., 1997b). EVI accounts for atmospheric effects and canopy background and is less prone to saturation, so it is often used in areas with dense vegetation (Huete et al., 1997a). NIRv is a recently developed indicator that overcomes the tendency of NDVI to saturate by multiplying NDVI by the near infrared band, which is highly sensitive to leaf cellular structure (Badgley et al., 2017). LSWI is computed using the shortwave infrared band, which is sensitive to leaf water and soil moisture (Xiao et al., 2002). These equations are as follows:

$$EVI = 2.5 \times \frac{NIR - RED}{NIR + 6*RED + 7.5*BLUE + 1} \tag{4}$$

$$NDVI = \frac{NIR - RED}{NIR + RED} \tag{5}$$

$$NIRv = NDVI \times NIR \tag{6}$$

$$LSWI = \frac{NIR - SWIR}{NIR + SWIR} \tag{7}$$

where *NIR* is the near infrared band, *RED* is the red band, *BLUE* is the blue band, and *SWIR* is the shortwave infrared band.

2.6 Copernicus Forest Cover

We used the 100-m Copernicus Land Cover dataset for the year 2019 (Buchhorn et al., 2020) to identify forest cover (data after 2019 is not available). For our analyses, we used only SIF soundings and MODIS pixels that fell within the forested areas. To help ensure that our spaceborne data were acquired over forest and to reduce the likelihood of mixed pixels and soundings with mixed land cover types, we converted the forest land cover raster data to polygon and created a 2.5 km inner buffer.

2.7 Ecoregions

We used the Terrestrial Ecoregions of the World boundaries (Olson et al., 2001) to distinguish between Africa's tropical forest types. We combined the Nigerian Lowland Forests and the Niger Delta Swamp Forest ecoregions, which are adjacent to each other, in our analyses due to the sparsity of forest and spaceborne data for these forests.

3 Results

We noticed that the wettest ecoregions also had the highest variability in monthly total rainfall, and that there was a dissimilarity in our results among the wettest ecoregions with a high variability in monthly precipitation and the drier ecoregions with low

variability. Thus, we classified the 11 ecoregions into three groups according to their precipitation regime, monthly variability, and mean annual rainfall (Table S1). Four ecoregions in West Africa were characterized by seasonalities that had distinctive single wet and dry periods each year, high monthly variability (sd ≥ 120 mm), and relatively high mean annual rainfall (> 2400 mm). We classified these ecoregions as West African moist tropical forest, which included the Cameroonian Highlands, Cross-Sanaga-Bioko Coastal Forest, Nigerian Lowlands and Niger Delta, and Western Guinean Lowlands. The six Central African ecoregions were characterized by seasonalities that typically had a double-peak pattern, low monthly variability (sd ≤ 100 mm), and relatively lower mean annual rainfall (< 2200 mm). We classified these forests as Central African tropical forests. The precipitation regime of the Eastern Guinean ecoregion in West Africa had mean annual rainfall (1544 mm) and monthly rainfall variability (81 mm) that was more similar to the Central African ecoregions.

3.1 West African moist tropical forests

3.1.1 Seasonality of SIF, environmental factors and VIs

We first evaluated the synchrony between SIF and precipitation for each ecoregion using lag correlations, and we found that the lag correlations were bimodal or plateaued for the West African moist tropical forests (Fig 1). SIF had a distinctive double-peak seasonality across all 11 ecoregions, but in the West African moist tropical forests the first peak in SIF was distinctively larger than the second and preceded peak precipitation (Fig. 2). SIF increased at the beginning of each year along with precipitation as temperature, PAR, and VPD decreased, but SIF peaked prior to peak precipitation and minimums in temperature, PAR, and VPD. The second, smaller peak in SIF tended to occur as precipitation decreased and PAR increased, but before large increases in VPD. Minimum SIF coincided with minimum precipitation and peaks in temperature, PAR, and VPD. PAR exhibited a relatively strong seasonality with minimums occurring mid-year due to high cloud cover during peak precipitation.
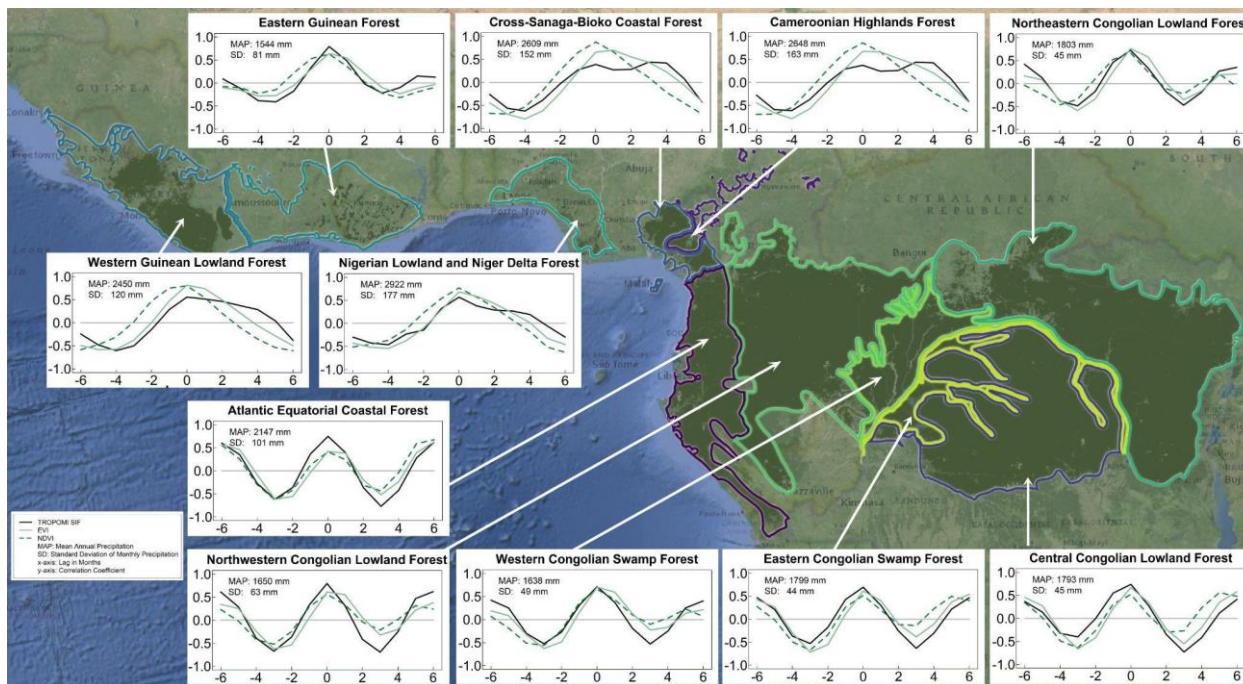
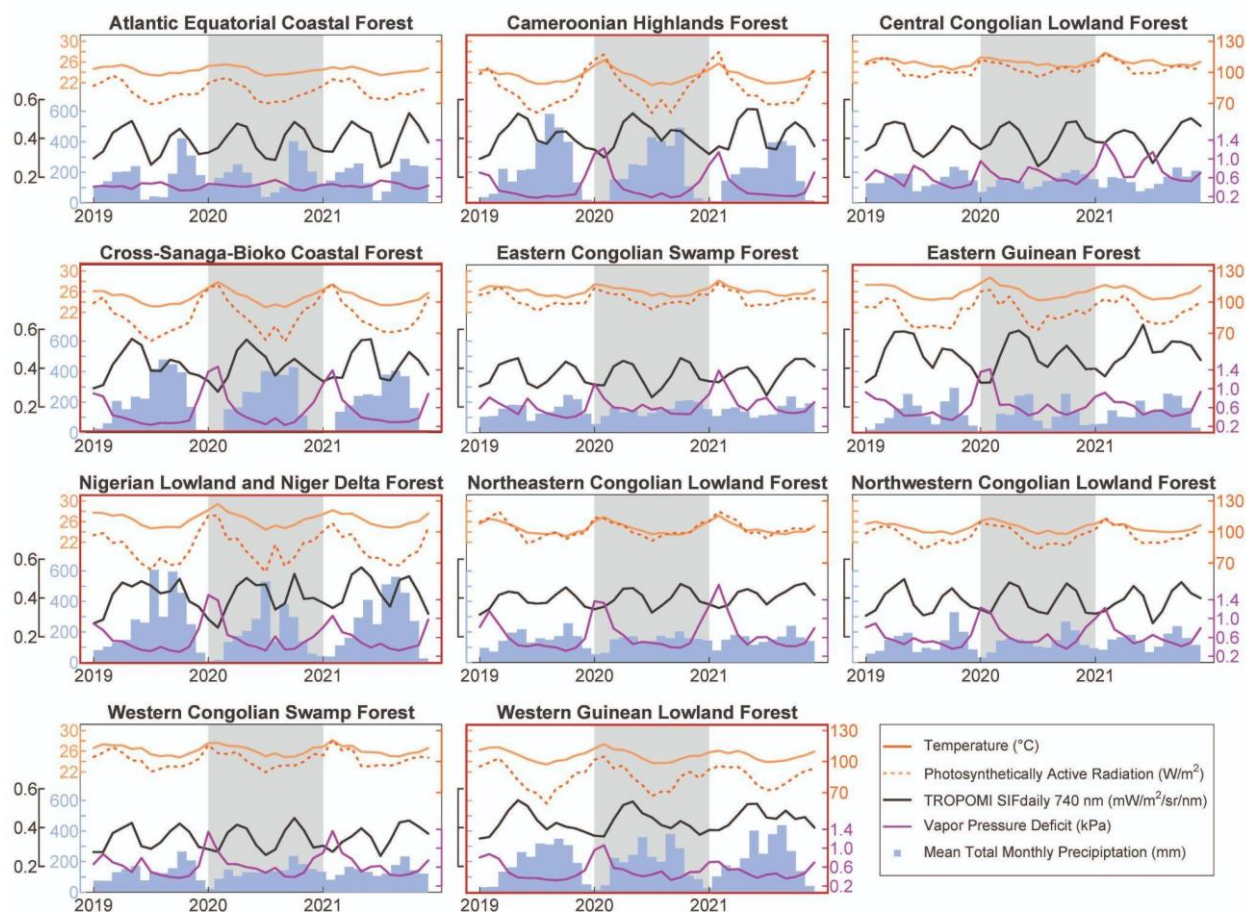**Figure 1. Lag correlation plots between precipitation and SIF, EVI, and NDVI for 11 tropical forest ecoregions. Positive values indicate a shift of the precipitation forward in time, and negative values indicate a shift of the precipitation backward in time.**

Fig. 2. Environmental conditions and solar-induced chlorophyll fluorescence for 11 African tropical forest ecoregions. Photosynthetically active radiation (PAR) is the amount of PAR at the top of the canopy (PAR$_{TOC}$). West African ecoregions are outlined in red.

NDVI and EVI did not mimic the double-peak seasonality we observed with SIF in the West African moist tropical forests (Fig. 3). Although SIF, NDVI, and EVI increased at the beginning of each year as precipitation increased, NDVI and EVI plateaued until substantial decreases in the dry season during the last quarter of the year.
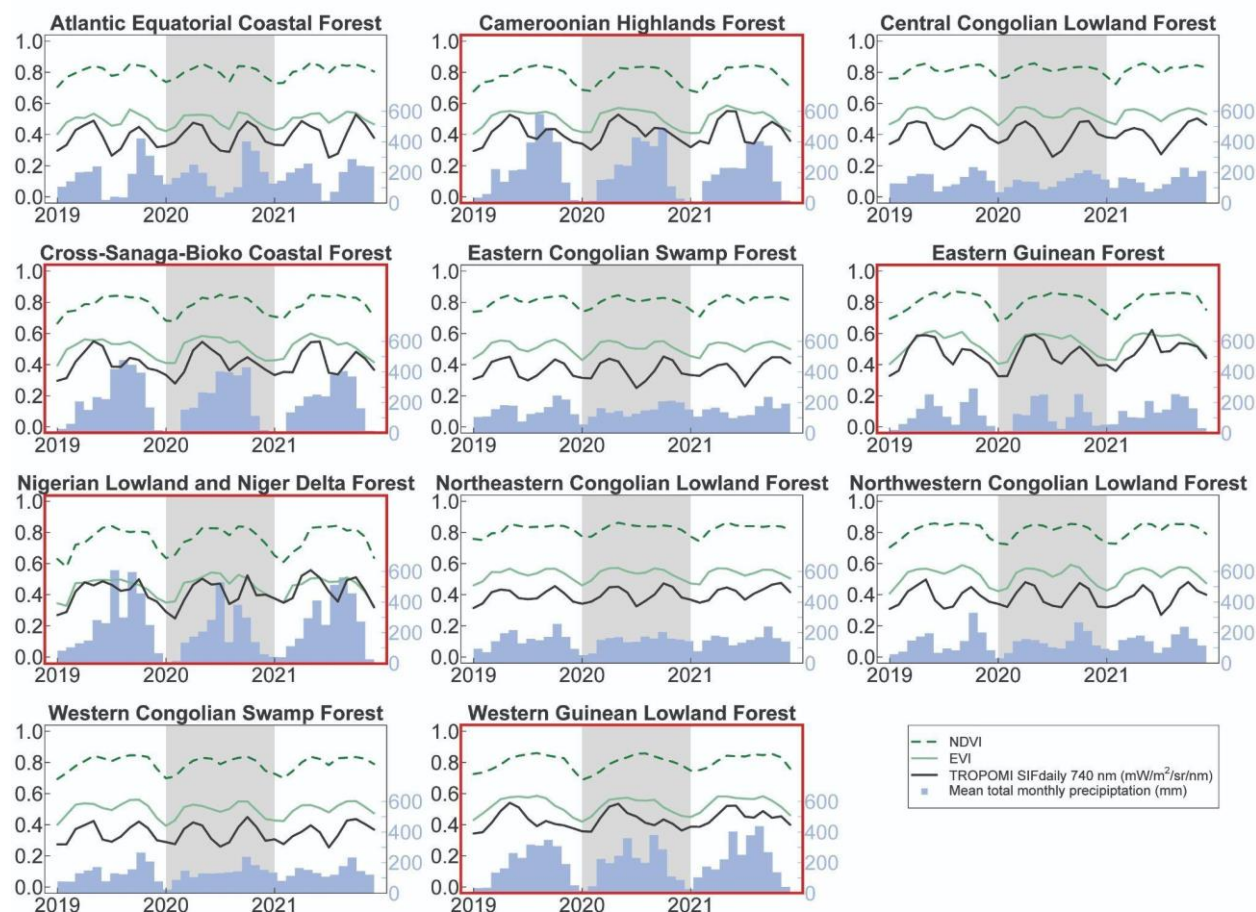
Figure 3. Monthly mean NDVI, EVI, SIF, and precipitation for 11 tropical forest ecoregions of Africa for 2019 - 2021. The shaded region delineates the year 2020. NDVI, EVI, and SIF share the left y-axis. West African ecoregions are outlined in red.

3.2 Central African tropical forests

3.2.1 Seasonality of SIF, environmental factors, and VIs

The seasonality of SIF and environmental factors in the Central African tropical forest differed remarkably from those in the West African moist tropical forest (Fig. 1). In Central Africa, the peaks and minimums in SIF tended to be similar in magnitude (Fig. 2) and were synchronous with precipitation, but there were some notable differences in the seasonalities of VPD. In the Atlantic Equatorial Coast Forest, VPD was relatively stable as the drier periods coincided with reduced temperature and PAR. In the Central Congolian Lowland Forest, VPD had a distinct double-peak seasonality that juxtaposed precipitation and SIF. In the four other Congolian ecoregions, there were large annual peaks in VPD that occurred at the beginning of the year when precipitation was low and temperatures high, but interestingly the magnitude of the decrease in SIF during this time was similar to the mid-year decrease in SIF when VPD was low.

203 Unlike the West African moist tropical forest, we found the seasonality of EVI to mimic SIF with a double-peak pattern in the
204 Central African tropical forest (Fig 3). The same was true for NDVI, except in the Northeastern Congolian Lowland where
205 NDVI plateaued during the wet season.

**3.2.2 Relationship between SIF, environmental factors and VIs**

207 When investigating the relationship between SIF and environmental factors, we found that SIF was significantly negatively
208 correlated with VPD in each ecoregion but was significantly positively correlated with precipitation (Figs. S1 and S2). The
209 correlations between SIF and VPD or precipitation were always higher than the correlations between SIF and temperature or
210 PAR, which were often insignificant, particularly in the Congo. These results were robust regardless of whether Pearson's or
211 Spearman's correlation was used for the analyses.

212 We found EVI, NIRv, and NDVI to also be negatively related to VPD across all sites, except for the Atlantic Equatorial Coastal
213 Forest where the relationships were not significant. Like SIF, these vegetation indices were positively associated with
214 precipitation in each ecoregion. The correlation between EVI, NIRv, and NDVI with temperature and PAR were generally
215 negative or insignificant across all sites.

216 When assessing whether SIF and the vegetation indices were more strongly correlated to VPD or precipitation at each site, we
217 found that the conclusion may depend on which correlation test was used. For instance, in the Nigerian Lowland and Niger
218 Delta Forest the Spearman's r for SIF and VPD was -0.73 and for SIF and precipitation r was 0.57, but when using Pearson's,
219 the r value was -0.65 and 0.66, respectively. Thus, when using Spearman's, one would conclude that SIF was more strongly
220 correlated with VPD than precipitation in this case, but when using Pearson's, one would conclude that the differences in the
221 correlations were negligible, so we reported correlation matrices for each method (Figs. S1 and S2).

222 However, when we compared differences in correlation coefficients for VPD and precipitation across all sites, we found that
223 the correlation between SIF and VPD strengthened and the correlation between SIF and precipitation weakened as mean annual
224 precipitation increased and the variability of monthly total precipitation increased (Fig. 4), regardless of whether Pearson's or
225 Spearman's correlation was used. Thus, SIF was increasingly related to VPD and less related to precipitation in forests with
226 higher annual total rainfall and higher variability in monthly precipitation. Conversely, we found NDVI to be increasingly
227 related to precipitation and less related to VPD in these same forests. However, this relationship is likely due to a saturated
228 NDVI signal that mimics the seasonality of precipitation in West African moist tropical forest, as no significant correlation
229 was found for EVI.

230
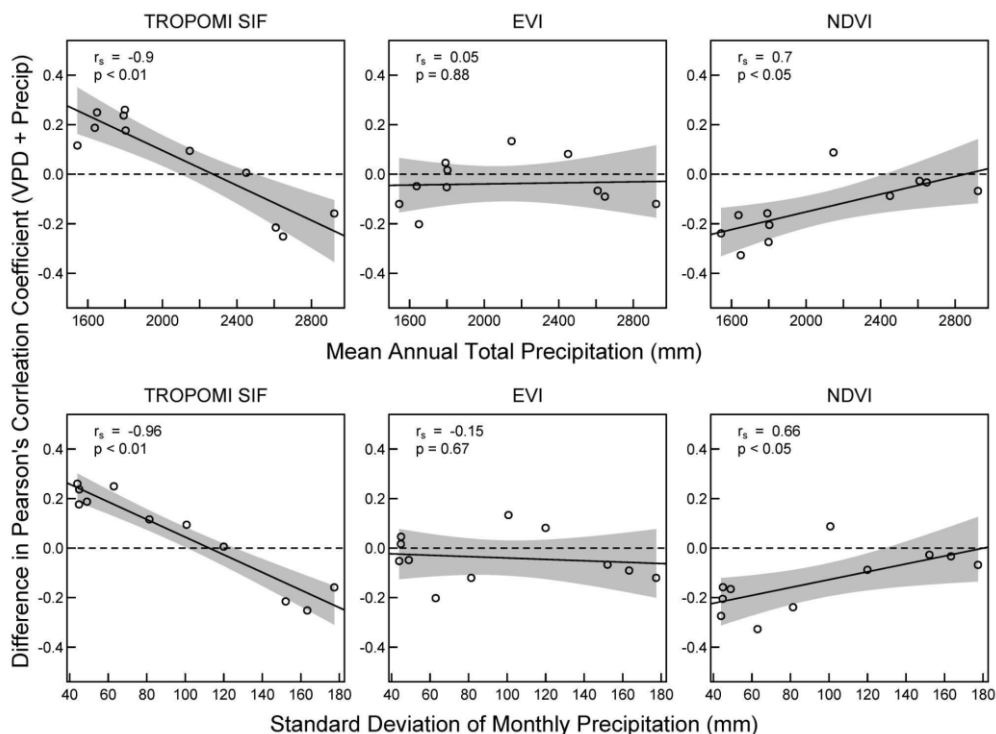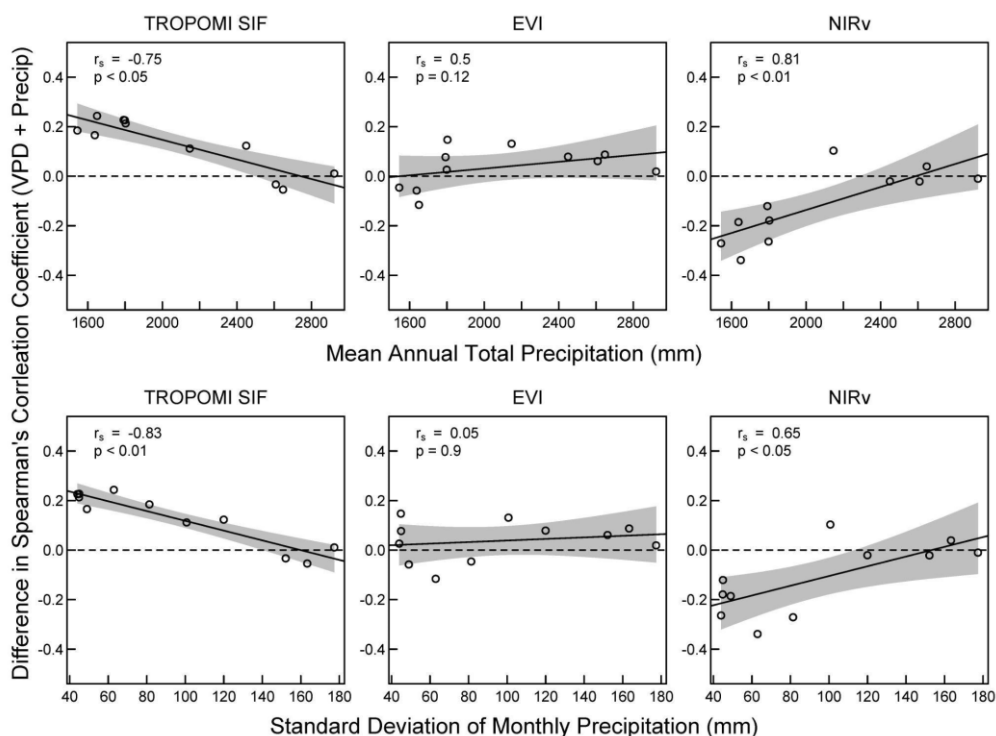
233 **Figure 4. Regressions of the differences in the correlation coefficients for SIF, EVI, and NDVI vs VPD and precipitation using**
234 **Pearson's and Spearman's correlation tests for each ecoregion. Differences are *r* for VPD minus *r* for precipitation. Top two rows**
235 **are differences in Pearson's correlation coefficient, and bottom two rows are differences in Spearman's correlation coefficient.**

236 **3.2.3 Synchrony in minimum and maximum SIF, EVI, and environmental factors**

237 The ecoregions of Central Africa straddle the equator, so we evaluated whether the double-peak seasonality in SIF, EVI, and

238 environmental factors were occurring locally, or whether the double peaks that we observed at the ecoregion scale were due

239 to the peaks alternating in time between the northern and southern regions. For SIF and EVI, we found that the double-peak

240 seasonality was largely a continental-scale phenomenon (Fig. 5, top two rows). Except for some forests at the northern and

241 southern most fringes, Central African tropical forests exhibited a double-peak seasonality in SIF and EVI.
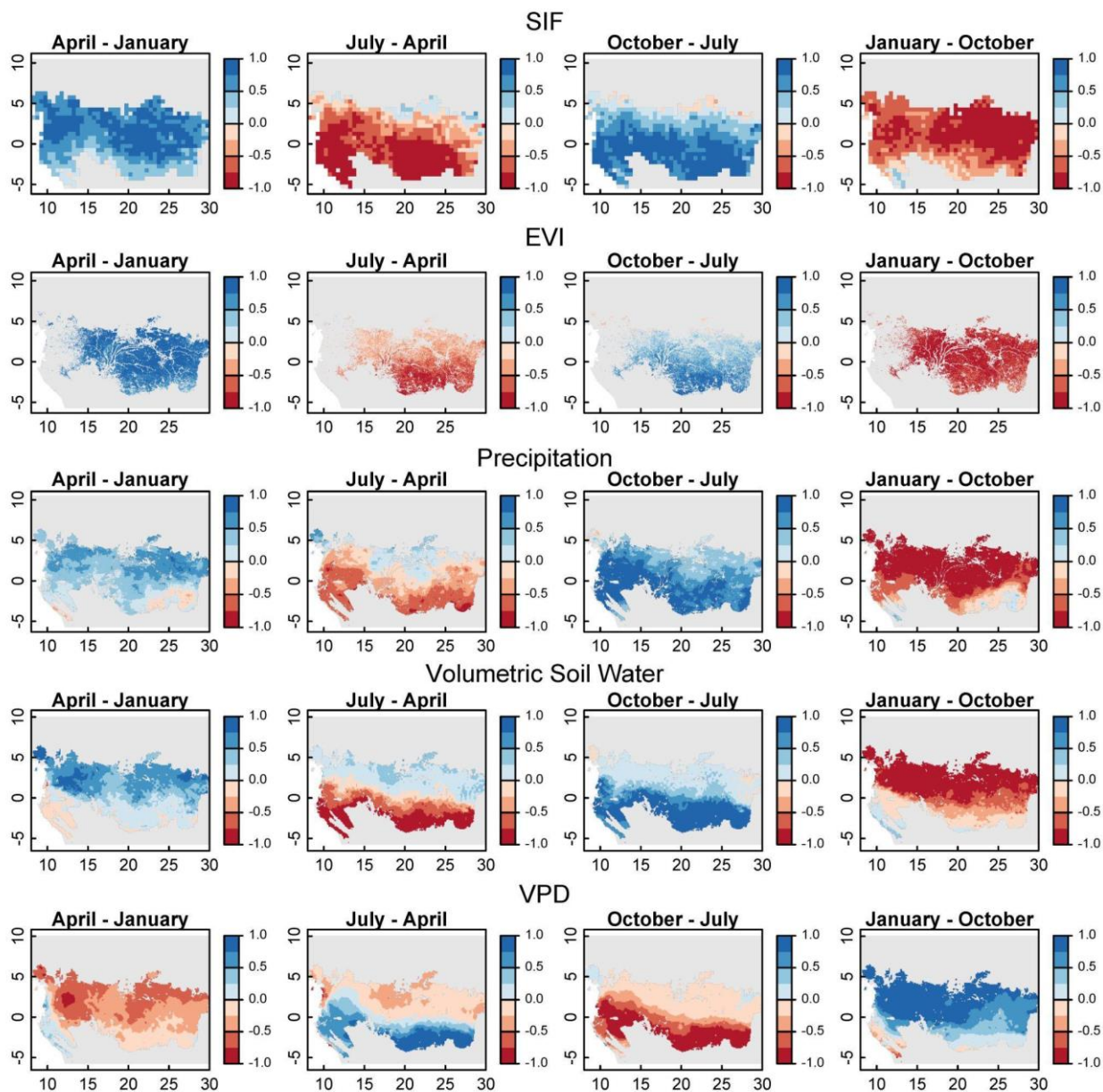
Fig. 5. Differences in normalized SIF, EVI, precipitation, volumetric soil water, and VPD. Shown are the changes from January to April (first column), April to July (second column), July to October (third column), and October to January (fourth column).

For precipitation, soil moisture, and VPD, the double-peak seasonality was mostly constrained to the southern portions of the Central African forest (Fig. 5, bottom three rows), with the northern regions more commonly experiencing increasing precipitation from January to April, April to July, and July to October with a single decrease occurring between October and January. These different precipitation regimes for the northern and southern regions of the Central Africa forests create a clear north-south divide in the timing of minimum SIF, EVI, precipitation, and soil moisture and maximum VPD (Fig. 6, first

column). In the northern region, these minimums and maximums in VPD occur in the beginning of the calendar year following

the southern solstice, and in the southern region they coincide with the mid-year northern solstice.

Interestingly, we did not find a similar bimodal north-south timing in maximum SIF, EVI, precipitation, soil moisture, or

minimum VPD. Maximum SIF and EVI had bimodal distributions, but these distributions did not have clear geographical

patterns. Maximum precipitation, soil moisture, and minimum VPD occurred nearly exclusively in the last quarter of the year.
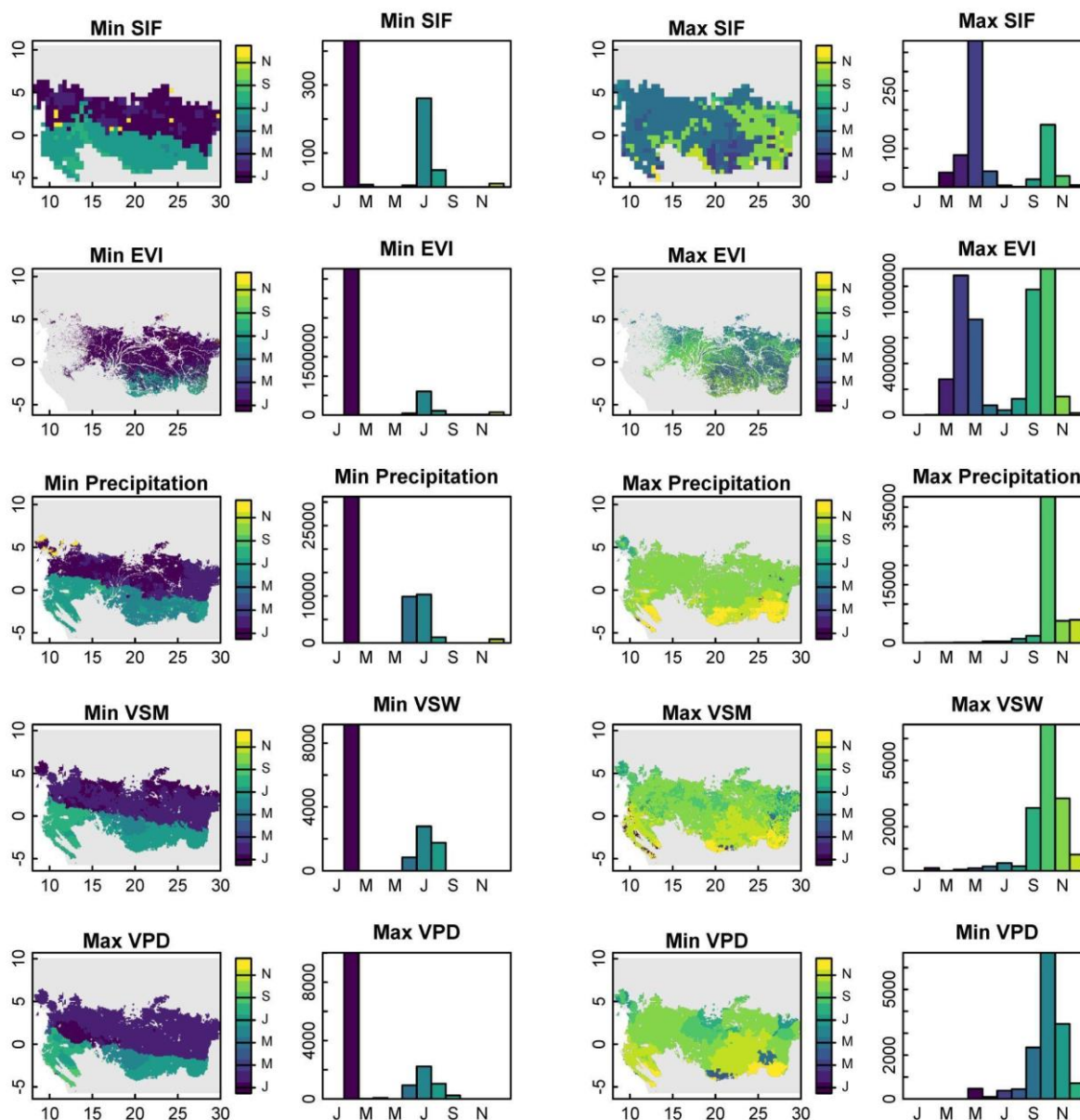

Fig. 6. Month in which minimum and maximum SIF, EVI, precipitation, volumetric soil water, and VPD occur in tropical African forests.

14

3.3 Robustness of the SIF signal

OCO-2 and OCO-3 agreed well with TROPOMI across an aggregate of the ecoregions, and the OCOs agree well with each other (Figs. 7 and S3). At the ecoregion level, the OCOs can better capture the seasonality of TROPOMI SIF in ecoregions with large intact forests due to a larger volume of OCO data at larger spatial scales, albeit with a slight high bias (Fig. S4). The higher bias of the OCO-2 and OCO-3 retrievals relative to TROPOMI could be related to the nadir viewing angle of the OCOs and differences in the retrieval windows, instrument characteristics, bias correction, and/or footprint size.
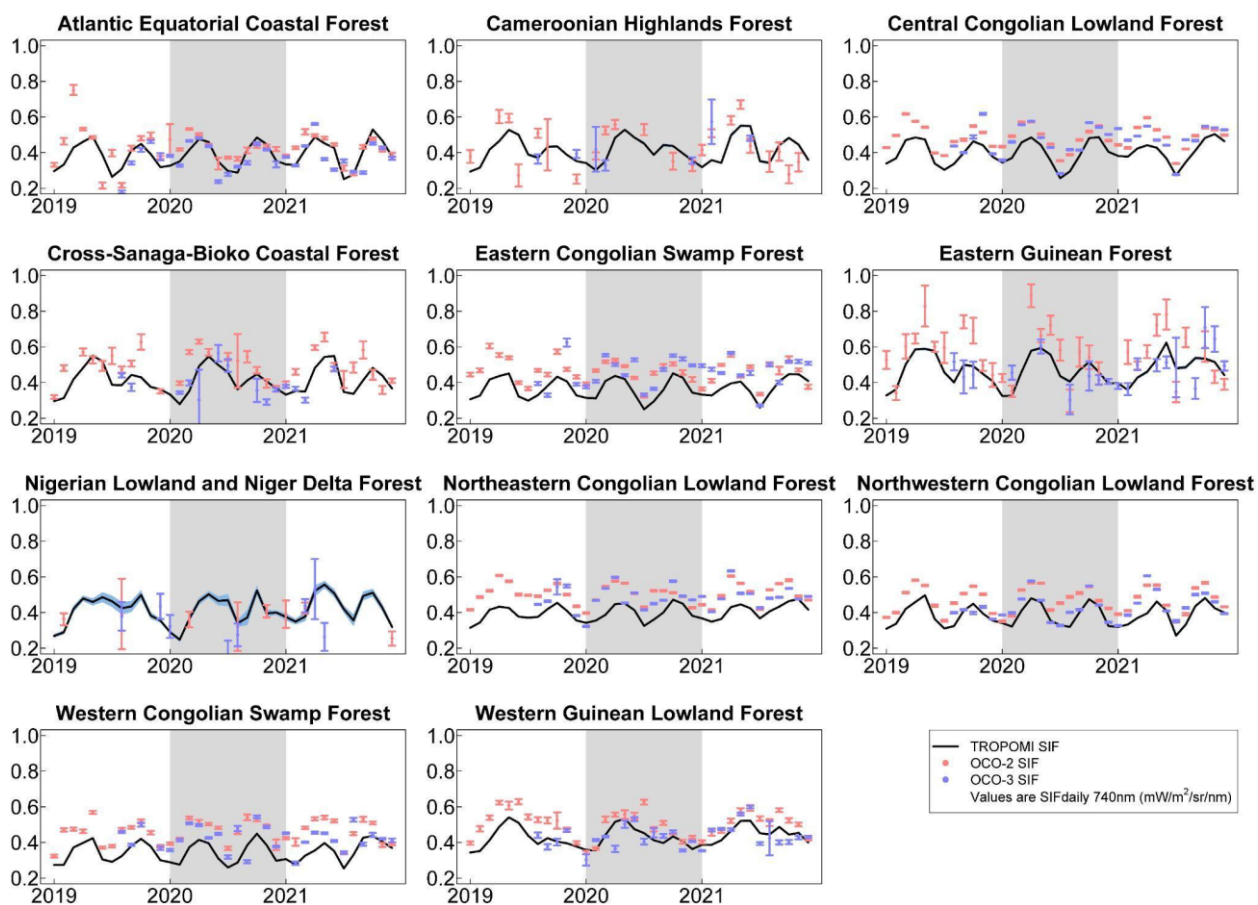
Fig 7. Monthly mean SIF from TROPOMI, OCO-2, and OCO-3 for 11 African tropical ecoregions for 2019 - 2021. OCO-2 and OCO-3 error bars and blue shaded region under the TROPOMI line are +/- the standard error of the mean. The shaded region delineates the year 2020.

4 Discussion

4.1 West African moist tropical forest

There were stark similarities in the timing of SIF, VIs, and precipitation in the moist Amazon and West African moist African forests, despite their apparent opposing responses to VPD. For both forest types, SIF and the VIs increased as precipitation increased after a distinct two- or three-month dry period, and SIF and the VIs peaked prior to peak precipitation and as PAR_{TOC} declined. These similarities indicate that there are similar changes in leaf physiology and demography in both the moist Amazon and West African moist tropical forests, with new leaf flush and increased productivity as the dry season is alleviated by increased rainfall.

However, we observed three main differences in the precipitation regimes of these West African moist forests and the Amazon forests. First, annual peak monthly precipitation for West African moist tropical forests was frequently as high as 400 mm - 600 mm, much higher than what has been observed in moist Amazon forests. These periods of intense rainfall in Africa cause reductions in PAR_{TOC} that are much larger than those seen in the Amazon, and may suppress $APAR_{chl}$, photosynthesis, and SIF as the ecosystem becomes light-limited. The alleviation of this light limitation in the weeks after peak precipitation could explain the second peak in SIF despite any noticeable changes in the VIs.

Second, the distribution of rainfall in a year was sometimes bimodal for the West African moist tropical forests, particularly for the Nigerian Lowland and Niger Delta Forest and the Western Guinean Lowland Forest, which likely contributed to the variability seen in the monthly SIF data for these ecoregions. Conversely, the precipitation regimes in the Amazon have been reported to be much less variable and are normally distributed (Liang et al., 2020).

Third, minimum precipitation in West African moist tropical forests occurs during the southern solstice around December, when the solar zenith angle and diffuse radiation is highest for that region, and maximum precipitation occurs between the northern solstice and southward equinox when PAR at the top of the atmosphere (PAR_{TOA}) is highest. Minimum and maximum precipitation for moist Amazon forests occurs during the southward and northward equinox, respectively.

Although we confirmed our first hypothesis that SIF in more moist ecoregions is less related to precipitation, we were surprised to find that SIF had a more negative relationship with PAR and VPD in West African moist tropical forests than those in Central Africa. We expected these forests to be radiation-limited rather than water-limited due to their high mean annual total rainfall. Instead, we found substantial decreases in SIF that were synchronous with increased PAR and VPD immediately following the wet season. These observations were contrary to what has been observed in the moist forests of the Amazon, where positive relationships exist between SIF, photosynthesis, and VPD due to newly flushed leaves during the dry season, which have higher photosynthetic capacity and compensate for stomatal closure due to increased VPD (Green et al., 2020; Wu et al., 2016). For West African moist tropical forest, our findings indicate that leaf abscission and leaf flush are synchronous with increasing and decreasing VPD.

4.2 Central African tropical forest

Correlative analyses of SIF, EVI, and environmental factors for Central African tropical forests at the continental or ecoregional scale indicate that SIF and EVI are synchronous with precipitation (Fig. 1). Such synchrony and high correlations allude that SIF and EVI, and thus the productivity of Central African tropical forests, are driven by precipitation. However, the drivers of the seasonality of SIF and EVI are much more complex.

For instance, we observed that the physiology and phenology of the entire Central African tropical forest region acts in concert, with a bimodal seasonality in SIF and EVI that occurs lockstep across the entire continent (Fig. 5, first two rows). This continental phenomenon occurs despite north-to-south differences in precipitation, soil moisture, and VPD regimes (Fig. 5, last three rows). Studies have shown that Central African tropical forests are extraordinarily resistant to precipitation anomalies (Asefi-Najafabady and Saatchi, 2013), long-term declines in annual total precipitation (Jiang et al., 2019; Malhi and Wright, 2004; Sun et al., 2022), and anomalies in the El Niño–Southern Oscillation and Madden–Julian Oscillation (Bennett et al., 2021; Raghavendra et al., 2020). Thus, the continental-scale bimodal seasonality of SIF and EVI are likely more related to solar insolation and angle than climate (Calle et al., 2010; van Schaik et al., 1993).

Nevertheless, the timing of minimum SIF and EVI are synchronous with minimum precipitation (Fig. 6, first two columns). Given the numerous studies that have highlighted the insensitivity of Central African tropical forests to precipitation anomalies, it is likely that the minimums in precipitation and solstice-related maximums in solar zenith angle serve as phenological queues for leaf abscission rather than directly inducing water-stress related declines in productivity. This explanation is supported by field observations, which found a north-south bimodal timing in peak leaf flush Central African tropical forests (van Schaik et al., 1993). Similarly, the timing of maximum SIF and EVI are likely less related to environmental factors (Fig. 6, last two columns) and could be more related to localized characteristics, such as herbivory, disturbance, topography, species composition, forest structure and age, soil characteristics, or other potential biotic and abiotic factors.

4.3 Future work

In deciduous ecosystems, SIF, photosynthesis, and vegetation indices are typically well correlated because both are driven by strong seasonalities in leaf area, canopy chlorophyll, and phenology (Doughty et al., 2021b). However, in evergreen ecosystems, including boreal needleleaf and tropical broadleaf, SIF and GPP can exhibit seasonal dynamics that do not well match vegetation indices because SIF and GPP are sensitive to changes in leaf demography, leaf physiology, and $APAR_{chl}$ (Doughty et al., 2021b, 2019; Gonçalves et al., 2020; Pierrat et al., 2022). For instance, it was found that spaceborne SIF had very low to no significant correlation with EVI and NDVI across tropical evergreen broadleaf forest in South America, Africa, and Southeast Asia (Doughty et al., 2021b), but that the seasonality of SIF in the Amazon and Africa well matched eddy covariance tower GPP (Doughty et al., 2019; Mengistu et al., 2021).

Anecdotally, we would expect the seasonality of SIF to also well match GPP in African tropical evergreen broadleaf forests, but such a comparison is not possible due to the absence of eddy towers in in-tact African tropical forests that are large enough

332 to not cause mixed-pixel effects with high temporal resolution satellite data. Ideally, a future eddy tower network in Africa

333 would be established in tropical forests across a precipitation gradient and include West African moist tropical forests and

334 Central African tropical forests. Litter-fall traps and phenology cameras at the tower sites would enable us to determine to

335 what degree observed changes in GPP are attributable to climate and leaf demography and physiology and could be directly

336 compared to spaceborne SIF and surface reflectance to validate our satellite observations.

337 Another topic that can be addressed is whether there is a significant long-term trend in SIF in the Central African tropical

338 forests, as it has been debated whether there is a browning trend in these forests (Sun et al., 2022; Zhou et al., 2014). As the

339 global spaceborne SIF record continues to lengthen over time, analyses of the SIF data records will allow us to not only address

340 whether there are long-term changes in greenness or leaf area but provide a clue as to whether there is a long-term trend in

341 photosynthesis. Similarly, the SIF data record has not yet been levered to address whether anomalies in SIF occur during

342 periods of La Nina or El Nino or during precipitation anomalies.

Data availability

344 All data used in our paper is publicly available. OCO-2 SIF Lite files can be accessed at

345 https://doi.org/10.5067/XO2LBBNPO010 (OCO-2 Science Team et al., 2020), and OCO-3 data can be accessed at

346 https://doi.org/10.5067/NOD1DPPBCXSO (OCO-3 Science Team et al., 2020). TROPOMI SIF can be accessed at

347 https://ftp.sron.nl/open-access-data-2/TROPOMI/tropomi/sif/v2.1/l2b/. CHIRPS Precipitation can be accessed at

348 https://data.chc.ucsb.edu/products/CHIRPS-2.0/. ERA-5 Reanalysis can be found at https://cds.climate.copernicus.eu/.

349 MODIS MCD43A4 data can be accessed at https://lpdaac.usgs.gov/products/mcd43a4v061/. Copernicus forest cover can be

350 accessed at https://land.copernicus.eu/global/products/lc. Terrestrial ecoregions can be accessed at

351 https://www.worldwildlife.org/publications/terrestrial-ecoregions-of-the-world.

Author contributions

353 RD and MW conceived this paper. RD and DW performed the analyses. RD prepared the paper with contributions from all

354 co-authors.

Competing interests

356 The contact author has declared that neither they nor their co-authors have any competing interests.

References

358 Asefi-Najafabady, S., Saatchi, S., 2013. Response of African humid tropical forests to recent rainfall anomalies. Philos.

359   Trans. R. Soc. B Biol. Sci. 368, 20120306.
360 Badgley, G., Field, C.B., Berry, J.A., 2017. Canopy near-infrared reflectance and terrestrial photosynthesis. Sci. Adv. 3,
361   e1602244.
362 Bennett, A.C., Dargie, G.C., Cuni-Sanchez, A., Tshibamba Mukendi, J., Hubau, W., Mukinzi, J.M., Phillips, O.L., Malhi, Y.,
363   Sullivan, M.J., Cooper, D.L., others, 2021. Resistance of African tropical forests to an extreme climate anomaly.
364   Proc. Natl. Acad. Sci. 118, e2003169118.
365 Blundo, C., Carilla, J., Grau, R., Malizia, A., Malizia, L., Osinaga-Acosta, O., Bird, M., Bradford, M., Catchpole, D., Ford,
366   A., others, 2021. Taking the pulse of Earth's tropical forests using networks of highly distributed plots. Biol.
367   Conserv. 260, 108849.
368 Buchhorn, M., Lesiv, M., Tsendbazar, N.-E., Herold, M., Bertels, L., Smets, B., 2020. Copernicus global land cover layers—
369   collection 2. Remote Sens. 12, 1044.
370 Calle, Z., Schlumpberger, B.O., Piedrahita, L., Leftin, A., Hammer, S.A., Tye, A., Borchert, R., 2010. Seasonal variation in
371   daily insolation induces synchronous bud break and flowering in the tropics. Trees 24, 865–877.
372 Doughty, R., Köhler, P., Frankenberg, C., Magney, T.S., Xiao, X., Qin, Y., Wu, X., Moore, B., 2019. TROPOMI reveals
373   dry-season increase of solar-induced chlorophyll fluorescence in the Amazon forest. Proc. Natl. Acad. Sci.
374   201908157.
375 Doughty, R., Kurosu, T., Parazoo, N., Köhler, P., Wang, Y., Sun, Y., Frankenberg, C., 2021a. Global GOSAT, OCO-2 and
376   OCO-3 Solar Induced Chlorophyll Fluorescence Datasets. Earth Syst. Sci. Data Discuss. 1–28.
377 Doughty, R., Xiao, X., Köhler, P., Frankenberg, C., Qin, Y., Wu, X., Ma, S., Moore III, B., 2021b. Global-scale consistency
378   of spaceborne vegetation indices, chlorophyll fluorescence, and photosynthesis. J. Geophys. Res. Biogeosciences
379   e2020JG006136.
380 Eldering, A., Taylor, T.E., O'Dell, C.W., Pavlick, R., 2019. The OCO-3 mission: measurement objectives and expected
381   performance based on 1 year of simulated data. Atmospheric Meas. Tech. 12.
382 Frankenberg, C., Fisher, J.B., Worden, J., Badgley, G., Saatchi, S.S., Lee, J.-E., Toon, G.C., Butz, A., Jung, M., Kuze, A.,
383   2011. New global observations of the terrestrial carbon cycle from GOSAT: Patterns of plant fluorescence with
384   gross primary productivity. Geophys. Res. Lett. 38.
385 Funk, C., Peterson, P., Landsfeld, M., Pedreros, D., Verdin, J., Shukla, S., Husak, G., Rowland, J., Harrison, L., Hoell, A.,
386   others, 2015. The climate hazards infrared precipitation with stations—a new environmental record for monitoring
387   extremes. Sci. Data 2, 1–21.
388 Gaubert, B., Stephens, B.B., Basu, S., Chevallier, F., Deng, F., Kort, E.A., Patra, P.K., Peters, W., Rödenbeck, C., Saeki, T.,
389   others, 2019. Global atmospheric CO 2 inverse models converging on neutral tropical land exchange, but
390   disagreeing on fossil fuel and atmospheric growth rate. Biogeosciences 16, 117–134.
391 Gonçalves, N.B., Lopes, A.P., Dalagnol, R., Wu, J., Pinho, D.M., Nelson, B.W., 2020. Both near-surface and satellite remote
392   sensing confirm drought legacy effect on tropical forest leaf phenology after 2015/2016 ENSO drought. Remote
393   Sens. Environ. 237, 111489.
394 Green, J., Berry, J., Ciais, P., Zhang, Y., Gentine, P., 2020. Amazon rainforest photosynthesis increases in response to
395   atmospheric dryness. Sci. Adv. 6, eabb7232.
396 Guan, K., Pan, M., Li, H., Wolf, A., Wu, J., Medvigy, D., Caylor, K.K., Sheffield, J., Wood, E.F., Malhi, Y., 2015.
397   Photosynthetic seasonality of global tropical forests constrained by hydroclimate. Nat. Geosci. 8, 284.
398 Guanter, L., Aben, I., Tol, P., Krijger, J.M., Hollstein, A., Köhler, P., Damm, A., Joiner, J., Frankenberg, C., Landgraf, J.,
399   2015. Potential of the TROPOspheric Monitoring Instrument (TROPOMI) onboard the Sentinel-5 Precursor for the
400   monitoring of terrestrial chlorophyll fluorescence. Atmospheric Meas. Tech. 8, 1337–1352.
401 Guanter, L., Bacour, C., Schneider, A., Aben, I., van Kempen, T.A., Maignan, F., Retscher, C., Köhler, P., Frankenberg, C.,
402   Joiner, J., others, 2021. The TROPOSIF global sun-induced fluorescence dataset from the Sentinel-5P TROPOMI
403   mission. Earth Syst. Sci. Data 13, 5423–5440.
404 Hubau, W., Lewis, S.L., Phillips, O.L., Affum-Baffoe, K., Beeckman, H., Cuní-Sanchez, A., Daniels, A.K., Ewango, C.E.N.,
405   Fauset, S., Mukinzi, J.M., 2020. Asynchronous Carbon Sink Saturation in African and Amazonian Tropical Forests.
406 Huete, A.R., Liu, H.Q., Batchily, K.V., van Leeuwen, W.J.D., 1997a. A comparison of vegetation indices over a global set
407   of TM images for EOS-MODIS. Remote Sens. Environ. 59, 440–451.
408 Huete, A.R., Liu, H.Q., van Leeuwen, W.J.D., 1997b. The use of vegetation indices in forested regions: issues of linearity

409   and saturation. Presented at the IGARSS'97. 1997 IEEE International Geoscience and Remote Sensing Symposium
410   Proceedings. Remote Sensing-A Scientific Vision for Sustainable Development, IEEE, pp. 1966–1968.
411 Jiang, Y., Zhou, L., Tucker, C.J., Raghavendra, A., Hua, W., Liu, Y.Y., Joiner, J., 2019. Widespread increase of boreal
412   summer dry season length over the Congo rainforest. Nat. Clim. Change 9, 617–622.
413 Johnson, J., Berry, J., 2021. The role of cytochrome b6f in the control of steady-state photosynthesis: a conceptual and
414   quantitative model. Photosynth. Res. 148, 101–136.
415 Köhler, P., Frankenberg, C., Magney, T.S., Guanter, L., Joiner, J., Landgraf, J., 2018. Global retrievals of solar induced
416   chlorophyll fluorescence with TROPOMI: first results and inter-sensor comparison to OCO-2. Geophys. Res. Lett.
417 Lawrence, D., Vandecar, K., 2015. Effects of tropical deforestation on climate and agriculture. Nat. Clim. Change 5, 27–36.
418 Liang, Y.-C., Lo, M.-H., Lan, C.-W., Seo, H., Ummenhofer, C.C., Yeager, S., Wu, R.-J., Steffen, J.D., 2020. Amplified
419   seasonal cycle in hydroclimate over the Amazon river basin and its plume region. Nat. Commun. 11, 4390.
420 Lopez-Gonzalez, G., Lewis, S.L., Burkitt, M., Phillips, O.L., 2011. ForestPlots. net: a web application and research tool to
421   manage and analyse tropical forest plot data.
422 Madani, N., Kimball, J.S., Jones, L.A., Parazoo, N.C., Guan, K., 2017. Global analysis of bioclimatic controls on ecosystem
423   productivity using satellite observations of solar-induced chlorophyll fluorescence. Remote Sens. 9, 530.
424 Magney, T.S., Barnes, M.L., Yang, X., 2020. On the covariation of chlorophyll fluorescence and photosynthesis across
425   scales. Geophys. Res. Lett. 47.
426 Malhi, Y., 2012. The productivity, metabolism and carbon cycle of tropical forest vegetation. J. Ecol. 100, 65–75.
427 Malhi, Y., Wright, J., 2004. Spatial patterns and recent trends in the climate of tropical rainforest regions. Philos. Trans. R.
428   Soc. Lond. B. Biol. Sci. 359, 311–329.
429 Mengistu, A.G., Mengistu Tsidu, G., Koren, G., Kooreman, M.L., Boersma, K.F., Tagesson, T., Ardö, J., Nouvellon, Y.,
430   Peters, W., 2021. Sun-induced fluorescence and near-infrared reflectance of vegetation track the seasonal dynamics
431   of gross primary production over Africa. Biogeosciences 18, 2843–2857.
432 Merbold, L., Ardö, J., Arneth, A., Scholes, R.J., Nouvellon, Y., De Grandcourt, A., Archibald, S., Bonnefond, J.-M.,
433   Boulain, N., Brueggemann, N., others, 2009. Precipitation as driver of carbon fluxes in 11 African ecosystems.
434   Biogeosciences 6, 1027–1041.
435 Monteith, J., Unsworth, M., 2013. Principles of environmental physics: plants, animals, and the atmosphere. Academic
436   Press.
437 Muñoz Sabater, J., 2019. ERA5-Land monthly averaged data from 1950 to present. Copernic. Clim. Change Serv. C3S Clim.
438   Data Store CDS. https://doi.org/10.24381/cds.68d2bb30
439 OCO-2 Science Team, Gunson, M., Eldering, A., 2020. OCO-2 Level 2 bias-corrected solar-induced fluorescence and other
440   select fields from the IMAP-DOAS algorithm aggregated as daily files, Retrospective processing VEarlyR.
441   Goddard Earth Sci. Data Inf. Serv. Cent. GES DISC. https://doi.org/10.5067/XO2LBBNPO010
442 OCO-3 Science Team, Gunson, M., Eldering, A., 2020. OCO-3 Level 2 bias-corrected solar-induced fluorescence and other
443   select fields from the IMAP-DOAS algorithm aggregated as daily files, Retrospective processing VEarlyR.
444   Goddard Earth Sci. Data Inf. Serv. Cent. GES DISC. https://doi.org/10.5067/NOD1DPPBCXSO
445 Olson, D.M., Dinerstein, E., Wikramanayake, E.D., Burgess, N.D., Powell, G.V., Underwood, E.C., D'amico, J.A., Itoua, I.,
446   Strand, H.E., Morrison, J.C., others, 2001. Terrestrial Ecoregions of the World: A New Map of Life on EarthA new
447   global map of terrestrial ecoregions provides an innovative tool for conserving biodiversity. BioScience 51, 933–
448   938.
449 Pan, Y., Birdsey, R.A., Fang, J., Houghton, R., Kauppi, P.E., Kurz, W.A., Phillips, O.L., Shvidenko, A., Lewis, S.L.,
450   Canadell, J.G., others, 2011. A large and persistent carbon sink in the world's forests. science 333, 988–993.
451 Pei, Y., Dong, J., Zhang, Y., Yuan, W., Doughty, R., Yang, J., Zhou, D., Zhang, L., Xiao, X., 2022. Evolution of light use
452   efficiency models: Improvement, uncertainties, and implications. Agric. For. Meteorol. 317, 108905.
453 Pierrat, Z., Magney, T., Parazoo, N.C., Grossmann, K., Bowling, D.R., Seibt, U., Johnson, B., Helgason, W., Barr, A.,
454   Bortnik, J., others, 2022. Diurnal and Seasonal Dynamics of Solar-Induced Chlorophyll Fluorescence, Vegetation
455   Indices, and Gross Primary Productivity in the Boreal Forest. J. Geophys. Res. Biogeosciences 127.
456 Porcar-Castell, A., Malenovskỳ, Z., Magney, T., Van Wittenberghe, S., Fernández-Marín, B., Maignan, F., Zhang, Y.,
457   Maseyk, K., Atherton, J., Albert, L.P., others, 2021. Chlorophyll a fluorescence illuminates a path connecting plant
458   molecular biology to Earth-system science. Nat. Plants 7, 998–1009.

459 Porcar-Castell, A., Tyystjärvi, E., Atherton, J., Van der Tol, C., Flexas, J., Pfündel, E.E., Moreno, J., Frankenberg, C., Berry,
460   J.A., 2014. Linking chlorophyll a fluorescence to photosynthesis for remote sensing applications: mechanisms and
461   challenges. J. Exp. Bot. 65, 4065–4095.
462 Raghavendra, A., Zhou, L., Roundy, P.E., Jiang, Y., Milrad, S.M., Hua, W., Xia, G., 2020. The MJO's impact on rainfall
463   trends over the Congo rainforest. Clim. Dyn. 54, 2683–2695.
464 Restrepo-Coupe, N., da Rocha, H.R., Hutyra, L.R., da Araujo, A.C., Borma, L.S., Christoffersen, B., Cabral, O.M., de
465   Camargo, P.B., Cardoso, F.L., da Costa, A.C.L., 2013. What drives the seasonality of photosynthesis across the
466   Amazon basin? A cross-site analysis of eddy flux tower measurements from the Brasil flux network. Agric. For.
467   Meteorol. 182, 128–144.
468 Rouse, J.W., Haas, R.H., Schell, J.A., Deering, D.W., 1974. Monitoring vegetation systems in the Great Plains with ERTS.
469 Schaaf, C., Wang, Z., 2015. MCD43A4 MODIS/Terra+ Aqua BRDF/Albedo Nadir BRDF Adjusted RefDaily L3 Global-
470   500m V006. NASA EOSDIS Land Process. DAAC.
471 Sitch, S., Friedlingstein, P., Gruber, N., Jones, S.D., Murray-Tortarolo, G., Ahlström, A., Doney, S.C., Graven, H., Heinze,
472   C., Huntingford, C., others, 2015. Recent trends and drivers of regional sources and sinks of carbon dioxide.
473   Biogeosciences 12, 653–679.
474 Spracklen, D.V., Arnold, S.R., Taylor, C., 2012. Observations of increased tropical rainfall preceded by air passage over
475   forests. Nature 489, 282–285.
476 Sun, Y., Knyazikhin, Y., She, X., Ni, X., Chen, C., Ren, H., Myneni, R.B., 2022. Seasonal and long-term variations in leaf
477   area of Congolese rainforest. Remote Sens. Environ. 268, 112762.
478 Umuhoza, J., Jiapaer, G., Tao, Y., Jiang, L., Zhang, L., Gasirabo, A., Umwali, E.D., Umugwaneza, A., 2023. Analysis of
479   fluctuations in vegetation dynamic over Africa using satellite data of solar-induced chlorophyll fluorescence. Ecol.
480   Indic. 146, 109846.
481 Van Deventer, H., Cho, M., Mutanga, O., Ramoelo, A., 2015. Capability of models to predict leaf N and P across four
482   seasons for six sub-tropical forest evergreen trees. ISPRS J. Photogramm. Remote Sens. 101, 209–220.
483 van Schaik, C.P., Terborgh, J.W., Wright, S.J., 1993. The phenology of tropical forests: adaptive significance and
484   consequences for primary consumers. Annu. Rev. Ecol. Syst. 24, 353–377.
485 Wang, X., Piao, S., Ciais, P., Friedlingstein, P., Myneni, R.B., Cox, P., Heimann, M., Miller, J., Peng, S., Wang, T., others,
486   2014. A two-fold increase of carbon cycle sensitivity to tropical temperature variations. Nature 506, 212–215.
487 Williams, C.A., Hanan, N.P., Neff, J.C., Scholes, R.J., Berry, J.A., Denning, A.S., Baker, D.F., 2007. Africa and the global
488   carbon cycle. Carbon Balance Manag. 2, 1–13.
489 Wu, J., Albert, L.P., Lopes, A.P., Restrepo-Coupe, N., Hayek, M., Wiedemann, K.T., Guan, K., Stark, S.C., Christoffersen,
490   B., Prohaska, N., 2016. Leaf development and demography explain photosynthetic seasonality in Amazon
491   evergreen forests. science 351, 972–976.
492 Xiao, X., Boles, S., Frolking, S., Salas, W., Moore Iii, B., Li, C., He, L., Zhao, R., 2002. Observation of flooding and rice
493   transplanting of paddy rice fields at the site to landscape scales in China using VEGETATION sensor data. Int. J.
494   Remote Sens. 23, 3009–3022.
495 Yang, K., Ryu, Y., Dechant, B., Berry, J.A., Hwang, Y., Jiang, C., Kang, M., Kim, J., Kimm, H., Kornfeld, A., 2018. Sun-
496   induced chlorophyll fluorescence is more strongly related to absorbed light than to photosynthesis at half-hourly
497   resolution in a rice paddy. Remote Sens. Environ. 216, 658–673.
498 Zhou, L., Tian, Y., Myneni, R.B., Ciais, P., Saatchi, S., Liu, Y.Y., Piao, S., Chen, H., Vermote, E.F., Song, C., others, 2014.
499   Widespread decline of Congo rainforest greenness in the past decade. Nature 509, 86–90.
500